Microchimica Acta
https://doi.org/10.1007/s00604-019-3233-z

ORIGINAL PAPER

A carbon dot and molecular beacon based fluorometric sensor for the cancer marker microRNA-21

Mohamad Mahani[1] · Zhahra Mousapour[2] · Faten Divsar[3] · Alireza Nomani[4] · Huangxian Ju[5]

Received: 28 September 2018 / Accepted: 4 January 2019

Abstract

A carbon quantum dot (CQD) labeled molecular beacon was synthesized and applied to the detection of microRNA-21. The CQDs possess low cytotoxicity, excellent water solubility, and photostability. The CQDs were characterized by transmission electron microscopy, dynamic light scattering, Fourier-transform infrared spectroscopy, and fluorescence spectroscopy. The molecular beacon (MB) was labeled with the CQDs at the 5′ end, and with Black Hole Quencher 1 (BHQ1) at the 3′ end. The two labels act as the donor and acceptor parts of a FRET system, respectively. Only weak fluorescence is observed in the absence of microRNA-21, and in the presence of scrambled or mismatched sequences. However, in the presence of microRNA-21, fluorescence intensity of the CQDs at 460 nm (excitation at 360 nm) recovers. The hybridization of the hairpin structure of the MB with microRNA-21 opens the loop of MB. Consequently, the distance between the BHQ1 quencher and the CQDs is increased and fluorescence changes. The probe has high sensitivity (with a 0.3 nM limit of detection) and specificity. It can distinguish between microRNA-21 and its single mismatch mutant and hence represents a valuable tool for the early cancer diagnosis.

Keywords Carbon quantum dots · Cancer detection · FRET · Fluorescence biosensor · BHQ1 quencher · Hairpin · Thermodynamic analysis

Introduction

MicroRNAs as short noncoding RNA molecules play a crucial role in the post-transcriptional regulation of gene expression [1]. The altered expression levels of microRNAs correlate with several cancer types, tumor stages and responses to treatments [2]. The role of microRNA in the development of cancer and its potential as early diagnostic and prognostic marker is to be determined [3–6]. However, precise study of the intracellular levels of microRNA is difficult due to their several properties, such as their slight sequence lengths, low abundance, ability to degradation, and little sequence variety among specific microRNA family members. To address these shortcomings, various techniques have been demonstrated for microRNA analysis, such as quantitative real-time PCR [7], RNA blotting [8], electrochemistry [9, 10], and microRNA microarray technology [11]. But, the problem is that majority of these methods show their best performance in homogeneous samples. Moreover, they usually have difficulty in live cell monitoring of expression and distribution of microRNA.

In situ fluorescent labeling technology is a simple, while effective alternative approach for live cell monitoring that shows a minimum interference with inhomogeneous nature of biological samples for intracellular microRNA detection [12]. However, fluorescent dyes can emit light only for a very short period of time due to photobleaching effect and thus can reduce the reliability in detection and quantification of

Electronic supplementary material The online version of this article (https://doi.org/10.1007/s00604-019-3233-z) contains supplementary material, which is available to authorized users.

✉ Mohamad Mahani
mahani@kgut.ac.ir

[1] Department of Chemistry, Faculty of Chemistry and Chemical Engineering, Graduate University of Advanced Technology, Kerman 7631818356, Iran

[2] Department of Nanotechnology, Faculty of Sciences and Modern Technologies, Graduate University of Advanced Technology, Kerman 7631818356, Iran

[3] Department of Chemistry, Payame Noor University, P. O. BOX: 19395-3197, Tehran, Iran

[4] Department of Pharmaceutics, Rutgers, The State University of New Jersey, Piscataway, NJ 08854-8020, USA

[5] State Key Laboratory of Analytical Chemistry for Life Science, Department of Chemistry, Nanjing University, Nanjing 210093, China

Published online: 01 February 2019

microRNA by this approach [13]. Instead of unstable fluorescent molecules, one can use carbon quantum dots (CQDs) as an appropriate source of fluorescent signal [14, 15]. CQDs are a class of nanostructured carbons can be obtained by low-cost fabrication techniques and have fascinating and important features such as good bio-compatibility, precise biological target, low toxicity, and stronger quantum size effect. Additionally, they show an incredible photostability and perfectly resist against photobleaching [16].

Special attention is paid to use CQDs in the Förster resonance energy transfer (FRET)-based techniques for probing complex intermolecular interactions. FRET describes radiation less energy transfer between two molecules, the donor fluorophore and the acceptor chromophore, through dipole-dipole coupling. This phenomenon is extremely distance-dependent and the spectral overlap between the donor emission and the acceptor absorption is mandatory. In previous work, we reported on a bimolecular-functionalized CQD that can detect the microRNA through FRET [17]. The FAM-labeled single stranded DNA molecule was adsorbed on the surface of carbon quantum dot which leads to the quenching of the green fluorescence due to FRET. In the presence of the complementary miRNA the fluorescence signal was recovered. The significant advantages of operation CQDs in FRET based biosensors for the challenging diagnostic demands is their great sensitivity, numerous capability, and homogeneous assay types [18, 19].

One of the popular CQD applications is through molecular beacon (MB) probes. MB is a hairpin-structured oligonucleotide probe with a fluorophore and a quencher group at each end of its molecular configuration. In the absence of target molecules ("off" state), MB is closed. Due to the quenching, at this state, only weak background fluorescence can be observed. Upon hybridization with the target, beacon conformation changes results hairpin opening and fluorescence is turned "on" showing a strong signal. The hairpin structure of MB is very sensitive and specific to the target molecules. The selectivity of MB is because of its peculiar hairpin that binding of a mismatched sequence to the loop makes the overall configuration thermodynamically unstable [20, 21].

In the present work, a carbon quantum dot molecular beacon structure with "signal-on" strategy is described for ultra-sensitive in vitro fluorimetric detection of microRNA-21. The carbon quantum dot was synthesized, first, by a convenient one-step synthesis method and then its fluorescent quantum efficiency was compared with a commercially available organic fluorophore. It was shown that at the "off" state (closed) of MB, the overlap between emission spectrum of the CQD and the absorption spectrum of Black hole quencher 1 (BHQ1) as a quencher molecule resulted in FRET mechanism, with a very weak fluorescent signal. Adding the microRNA-21 molecules to the sample lead to opening the MB stem and separating the CQD and quencher from each other, consequently CQD's fluorescence emission can be observed.

Experimental

Chemicals and reagents

Ascorbic acid, sodium chloride, magnesium chloride, disodium hydrogen phosphate dihydrate and potassium dihydrogen phosphate were purchased from Merck (Merck Co., Darmstadt, Germany, www.merckmillipore.com). BHQ1, N-(3-dimethylaminopropyl)-N′-ethyl-carbodiimide hydrochloride (EDC), N-hydroxysuccinimide (NHS) and Quinine hemisulfate were obtained from Sigma-Aldrich (Sigma-Aldrich Co., Saint Louis, Missouri, USA, www.sigmaaldrich.com). The oligonucleotide sequences were purchased from Bioneer (Bioneer Co., South Korea, http://eng.bioneer.com) and used without further purification. The used sequences for the DNA strands are shown in Table S1.

Apparatus

The size distribution and zeta potential of CQDs were characterized by Zetasizer NanoZS90 (Malvern Instruments Ltd., Malvern, Worcestershire, UK, www.malvern.com) at 25 °C. The morphology and particle size of the CQDs were also studied by transmission electron microscopy (TEM, Hitachi, Japan). For TEM imaging, the sample was placed on a copper grid and dried under vacuum. The surface functional properties were investigated by Bruker TENSOR 27 FTIR spectrometer (Bruker Optics GmbH, Ettlingen, Germany, www.Bruker.com), and the optical absorption and fluorescence spectra of the fabricated CQDs were investigated by Varian Cary 50 UV-Vis spectrophotometer (Varian Co., Australia) and Varian Cary Eclipse Fluorescence Spectrophotometer (Varian Co., Australia).

Preparation of the carbon quantum dots (CQDs)

The synthesis of carbon quantum dots was performed according to the previously reported single-step hydrothermal method [22, 23]. The quantum yields of CQDs was determined by comparison of the wavelength integrated intensity of CQDs to that of the quinine sulfate in 0.1 M H_2SO_4 ($\Phi_F = 0.54$) as the standard control [24]. The 3-(4,5-dimethylthiazol-2-yl)-2,5-diphenyl-2H-tetrazolium bromide (MTT) assays were used to determine the cell viability after treatment by the CQDs. See the electronic supplementary materials (Section 1 to 3) for synthesis procedure, quantum yield calculations and MTT assay.

Preparation of the MB-CQD conjugate

In the optimized condition for preparation of the sensing probe, 0.5 mL of the CQD solution in 0.5 mL PBS buffer (containing 20 mM NaCl, and 10 mM $MgCl_2$, pH 7.4) was activated using 5 μL of 50 mM EDC and 5 μL of 50 mM NHS. The mixture was stirred for 15 min at room temperature, while protected from light. 100 μM of NH_2-MB-BHQ1 was added into the mixture and stirred for two hours at room temperature. In this reaction, the surface carboxyl groups of the CQDs and the amino groups of NH_2-MB-BHQ1 will be conjugated by amide linkage. Finally, the unconjugated reagents were removed by centrifugation at 12000 rcf for 30 min and then the fluorescence spectra of CQDs and the CQD-MBs were recorded.

Detection of the microRNA-21

Hybridization experiments were carried out in a 50 mM PBS buffer (pH 7.4). Twenty microliters of the CQD-MB-BHQ1 conjugate (6 μM) was mixed with different amounts of the microRNA-21 (up to 2 μM) in a total volume of 200 μL. After 20 min incubation at ambient conditions, the fluorescence of the mixture was measured for detection of varying FRET efficiency. Single mismatch or scrambled microRNAs were also measured as the control.

Results and discussion

MicroRNA-21, as an example of microRNAs, constitutes only a very diminutive portion of cellular total RNAs and because of that, the early detection of microRNA-21 as a cancer biomarker in human serum requires a very sensitive detection approach. We have designed a biosensor for detecting the microRNA-21 without preconcentration or other additional sample processing steps. The general principle behind the turn-on fluorescent microRNA-21 sensing platform is illustrated in Fig. 1. The main applied mechanism is based on the FRET theory which is supposed to occur between CQDs and BHQ1 at the end of dual-fluorophore-based MB.

Choice of materials

The choice of CQDs as a fluorophore is due to their broad absorption with narrow and tunable emission spectra which have made them excellent donors for FRET based biosensors. CQDs are becoming more desirable alternative than metal-based QDs and dye probes owing to their high biocompatibility, low toxicity, ease of preparation, and unique photophysical properties.

In comparison to organic dyes, CQDs have excellent photostability against photo bleaching, small size with diameters less than 10 nm, and exceptional multi-photon excitation property. However, metal-based QDs are associated with long-term toxicity and environmental concerns owing to the use of heavy metals. In addition complex procedures are required to obtain metal-based QDs, and their aggregation is often observed after long-term storage. CQDs do not have the toxic effect observed from heavy metals because CQDs contain large amounts of carbon and relatively low amounts of oxygen, hydrogen, and nitrogen. Moreover, CQDs have very strong blinking than other fluorescent metal-based QDs.

Characterization of CQDs

Figure 2a shows the TEM image of the CQDs. This representative TEM image shows that the CQDs are spherical particles with a normal distribution and a maximum size frequency at 1.0 nm. Additionally, the hydrodynamic diameter of this CQD was measured by Zetasizer (Fig. 2b) which shows the particle size of about 2 ± 1 nm. The size stability testing results showed that the average size of the CQDs did not change significantly after one-month incubation at 4 °C.

In addition, the FTIR spectrum of the CQDs was recorded to achieve additional structural insights about them (Fig. 2c). The characteristic absorption bands of O − H at 3408 cm^{-1}, the stretching vibration band of C=O at 1702 cm^{-1}, and the stretching vibration bands of C − O at 1000 and 775 cm^{-1} demonstrate the presence of carboxylic acid and other similar oxygen-containing functional groups [25]. Moreover, three apparent absorption peaks at 2927, 1391 and 1210 cm^{-1} are related to the stretching vibrations of C − H, C=C and C − C groups, respectively, indicating the existence of alkyl and aryl groups in the CQDs' structure [26].

Toxicity of CQDs

The toxicity of the carbon quantum dots was investigated by MTT assays. To determine the cytotoxicity of CQDs, different concentrations of CQDs from 0.25 to 10 $\mu g.mL^{-1}$ were treated with MCF-7 cells for 24 h. As shown in Fig. S1, there is a mild reduction in the viability of cells with increasing concentrations of CQDs. The treated cells displayed viabilities more than 90% of the tested concentration range. The estimated IC50% was about 58 $\mu g.mL^{-1}$ for this CQD. These results suggested that CQDs did not impose a considerable toxicity towards MCF-7 cells as compared to the control [17] and can be used as a safe and promising probe for bio imaging and cell labeling.

Optical properties of the CQDs and of Black Hole Quencher 1 (BHQ-1)

In the next step, the general optical properties of the CQDs, such as UV absorption and fluorescence emission spectra were

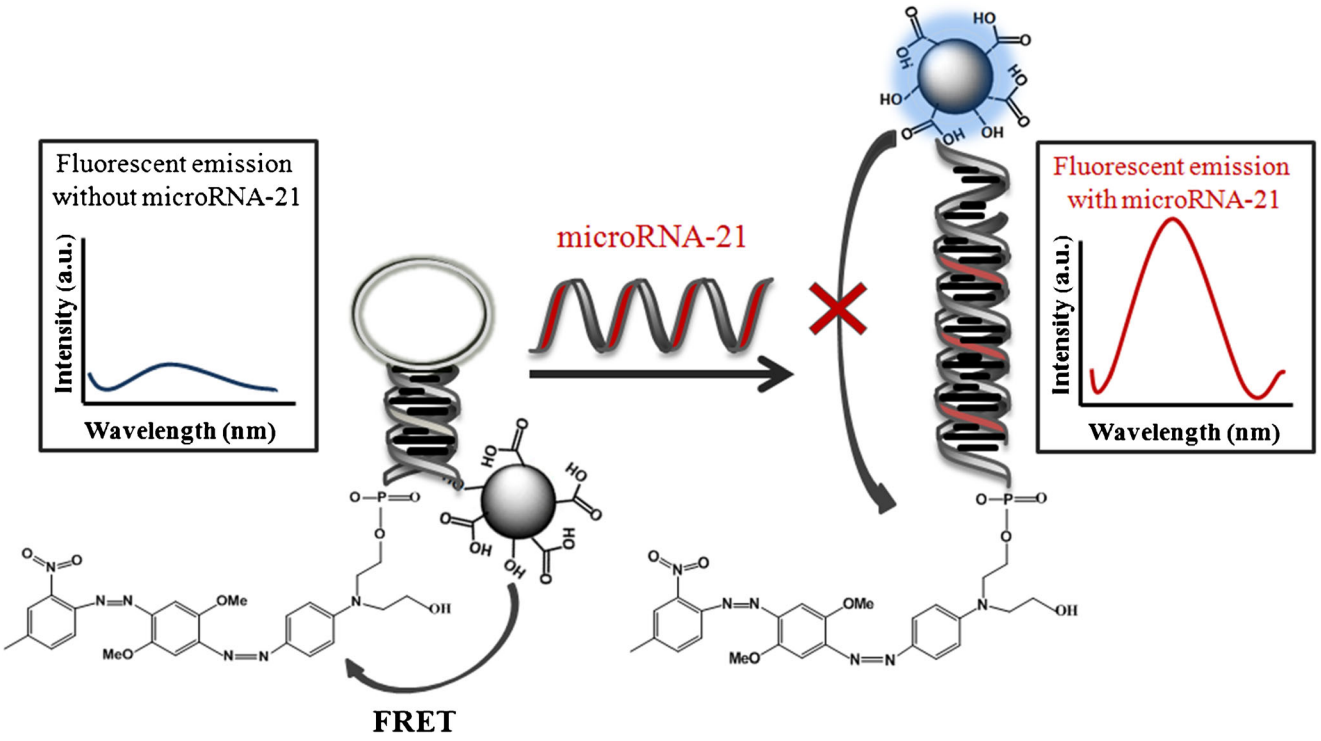

Fig. 1 Turn-on fluorescent microR-21 sensing platform using carbon dots and a black hole quencher of their fluorescence

evaluated (Fig. S2). The UV-Vis absorption spectrum (Fig. S2A) was obtained in the range of 270 nm to 580 nm. The maximum absorbance of CQDs occurred at 360 nm, corresponding to the typical absorption of an aromatic moiety having an sp^2 carbon network and the $n \rightarrow \pi^*$ transition of carbonyl groups [27]. Additionally, the well-dispersed aqueous suspension of CQDs exhibited a bright blue emission when exposed to the UV light.

Figure S2B shows the emission spectra of the CQDs at various excitation wavelengths. In general, the fluorescence emission spectra of this CQD show a symmetric Gaussian feature. At 360 nm excitation, a broad emission peak centered at 460 nm was observed in the emission spectrum. Figure 4b represents the excitation dependent fluorescence of the CQDs which reflects the effect of different size particles in the sample and a distribution of different surface states [28–30]. As shown in FTIR, the CQDs have various functional groups, on the surface which may result in a series of emissive traps between π and π^* states. With different excitation wavelengths, various surface state scattered traps will become dominant and the luminescence mechanism is controlled by both size effect and surface defect. In case of surface functionalization, the CQDs also show a slight red shift of the maximum emission peak at around 440 to 460 nm (Fig. S3).

The next evaluated important optical property was the quantum yield (QY). To calculate the QY of the CQDs, the fluorescence intensity of CQDs and quinine sulfate (as the standard control, which had a QY of 54%) was recorded at five different concentrations. The concentrations of CQDs and quinine sulfate were indicated indirectly by their absorbances. The resulting linear regression equations are also shown in

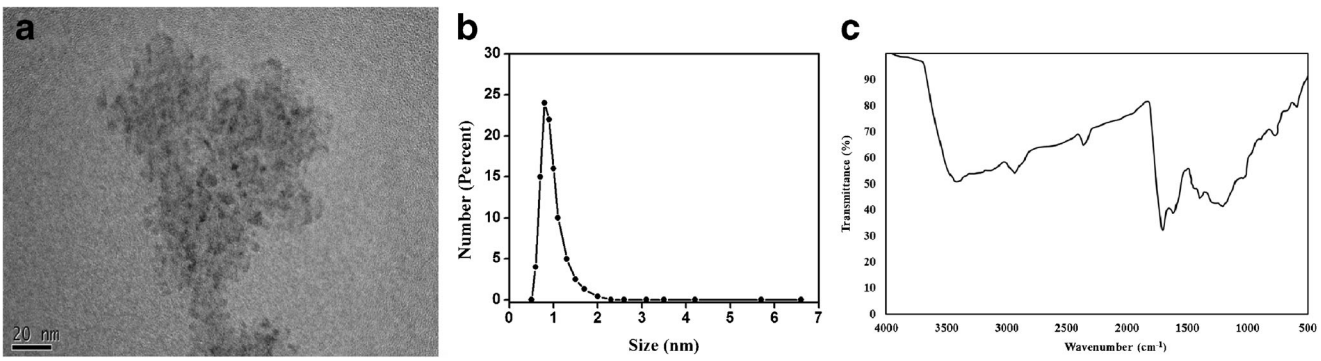

Fig. 2 **a** TEM image, **b** Hydrodynamic diameters of the CQDs and (**c**) FTIR spectrum of the CQDs

Figs. S4A and B. According to the mentioned QY calculation equation, the QY of the CQDs was estimated to be about 2.2% which is comparable to the previous reports [31, 32].

Next we evaluated the UV-Vis absorption spectrum of BHQ1 and fluorescent emission spectrum of CQDs. Figure 3 shows that the maximum absorption wavelength of BHQ1 and the emission wavelength of CQDs are 534 and 460 nm, respectively. The effective excited energy transfer from QDs to BHQ1 based on the Förster resonance energy-transfer (FRET) mechanism can occur due to the acceptable spectral overlap between the absorption spectra of BHQ1 and the emission spectra of QDs.

Bioconjugation of molecular beacon (MB) to the surface of CQDs

The reactivity of CQDs is strongly influenced by the characteristics of their surface groups. Oxygen atoms in the form of carboxylic acid groups make the surface of CQDs hydrophilic and helps them for a proper dispersion in water. To access the acidic groups on the surface of CQDs, Boehm method, which is an acid-base titration assay, was applied [33]. Using this method, the number of acidic surface groups was calculated from the consumed amount of sodium hydroxide which neutralizes CQDs carboxyl groups. In this procedure, 0.5 mL of the CQD solution was titrated with 0.5 M NaOH solution. As shown in Fig. S5, the equivalence point was reached at pH 5.8 by adding 0.56 ml of NaOH. According to this titration, the carboxylic acid residues on the carbon dots surface were found to be 0.28 mmol which was then activated by 0.28 mmol EDC and NHS with a molar ratio 1:1 of EDC:COOH and 1:1 of NHS:COOH. After that the activated carboxylic acid groups were reacted with the designed primary amine-containing molecular beacon.

Environmental pH value also influences the MBs function [34]. High pH value can break down the stem section and causes the degeneration of MBs which leads to a false-positive result. Because of that, we decided to perform all of the experiments in PBS buffer at pH 7.4.

The fluorescent spectra of CQDs, before and after conjugation with MB are shown in Fig. S6. In the absence of complementary target, the MB designs a partial duplex beacon and stays in the quenched state. This is due to the fact that the BHQ1 section is located in the close proximity of the CQDs structure and thus the fluorescence intensity of CQDs will be significantly quenched (Fig. S6b). The binding of microRNA-21 to the beacon induces a long distance between the BHQ1 and the CQD and therefore we can observe a remarkable return and enhancement in the CQDs' fluorescent signal (Fig. S6c).

This initial experimental data showed that the designed biosensor worked well for detecting microRNA-21.

Limit of detection and selectivity of the assay

Figure 4a shows the steady-state fluorescence emission spectra of the biosensor at various concentrations of the microRNA-21 in PBS. This result shows an appropriate correlation between microRNA-21 concentration and fluorescent emission of the designed QDs-MB-BHQ1 at 460 nm (Fig. 4b). Considering a broad concentration range of microRNA-21 (between 5 and 160 nM) a neat linearity was observed with a linear equation of $y = 1.1407x + 58.37$. The R value for the linear regression was 0.9962. Moreover, the LOD of the biosensor was 0.3 nM of microRNA-21 which was determined by the equation $LOD = 3\sigma/s$, where σ is the standard deviation of three measurements of blank solutions, and s is the slope of the calibration plot.

Comparison of the present study with other methods is shown in Table S2. From this table, we can see that the limit of detection of our assay method is comparative to the previously reported assays.

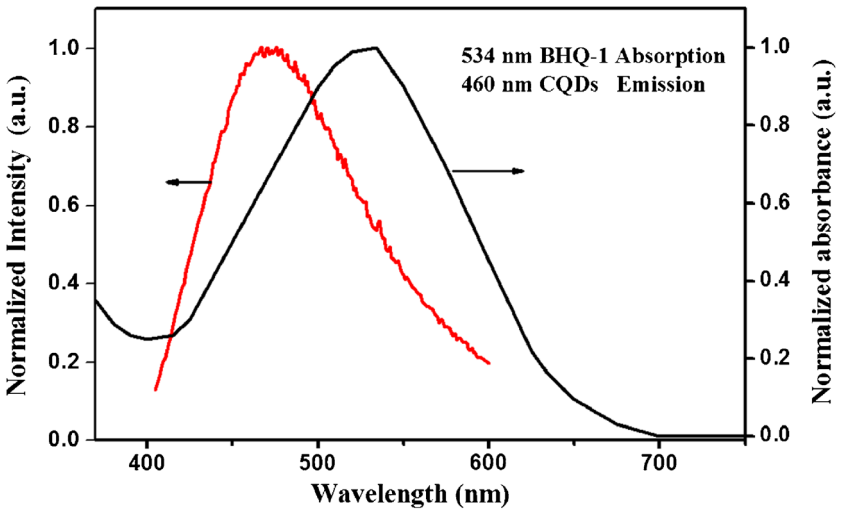

Fig. 3 Spectral overlap between FRET donor-acceptor pair. Emission spectrum of the CQDs-donor (left profile with 460 nm emission peak resulted from 360 nm excitation) and absorption spectra of BHQ-1-acceptors (Right profile with 534 nm absorption peak)

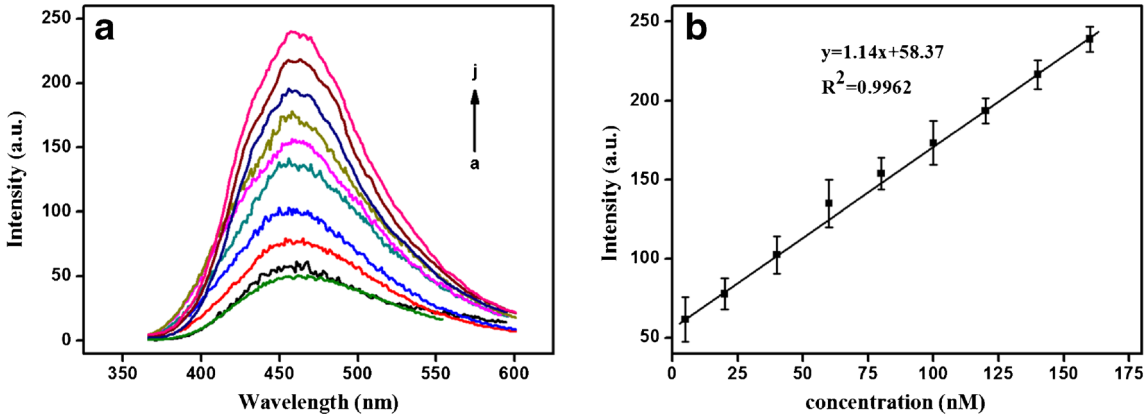

Fig. 4 **a** Fluorescence intensity of CQD-MB-BHQ1 after incubation with different concentration of the target microRNA-21 (a-j) 0, 5, 20, 40, 60, 80, 100, 120, 140, 160 nM. **b** Calibration plot of the peak fluorescence intensity at 460 nm (360 nm excitation wavelength) against microRNA-21 concentration in 50 mM PBS buffer (pH 7.4). The error bars are standard deviations of three repeated measurements

The specificity of the biosensor was evaluated in the presence of complementary target, single-base mismatched and scrambled (non-complimentary) strands at a similar sequence concentration. As shown in Fig. 5, we can see an intense increase at the biosensor's fluorescence emission in the presence of the complementary target DNA sequence. The microRNA-21 can enhance the fluorescence emission of the biosensor up to five folds compared to the basic emission in the absence of any sequence. On the other hand, the scrambled sequence failed to induce any significant change at the emission of the CQD biosensor. Even a single mismatch caused around 20% lower fluorescence intensity compared to the microRNA-21. These results suggest that the biosensor has great sequence specificity toward the microRNA-21.

Thermodynamic analysis of the biosensor

The thermodynamic property of molecular beacon is depended on its individuality and certain sequence of bases in the single-strand loop region which is complementary to the target sequence. The structure of the stem region also plays a significant role in the stability of the hairpin. The Gibbs Free Energy (ΔG) calculates the amount of reversible work that may be carried out at a constant temperature. The stability of hairpin is commonly characterized by its ΔG value that shows the quantity of energy needed to break the bonds and change the MB conformation. More negative number for ΔG shows primer self-dimer and more stable hairpins.

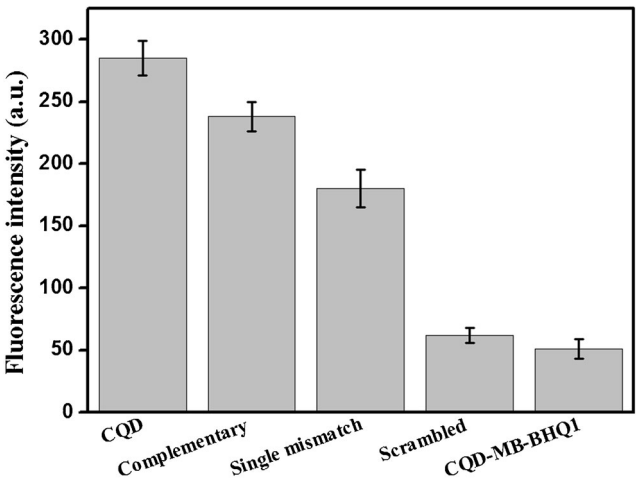

Fig. 5 Specificity of CQD-MB-BHQ1 biosensor for its target sequence. The biosensor was incubated with 160 nM target miR-21, single mismatch and scrambled sequences at the similar concentrations

The hairpin structure was utilized to overcome the specificity limitation of the oligonucleotide probes as the length of the probe is increased. The stem length of the hairpin is still a limitation and too long-stem-hairpin tend to closed in the presence of target due to slow hybridization kinetics.

Herein, the ΔG calculation of primers was performed by Gene runner software. The satisfactory value of −5.64 kcal.mol^{-1} was obtained for 3'end self-dimer that refers to intermolecular interactions within the primer and stable hairpin formation (Table 1). The ΔG values of −1.09 and 2.36 kcal.mol^{-1} were obtained for complementary and mismatch microRNA-21 respectively which confirmed hairpin structure was not formed for these sequences. In the case of intermolecular interactions between the same sense primers, ΔG values of −16.94, −6.60 and −3.61 kcal.mol^{-1} were achieved for molecular beacon, complementary and mismatch microRNA-21 which indicates possibility of formation their self-dimer conformation.

Table 1 Gibbs free energy data of hairpin and self-dimer conformations

Oligonucleotide	ΔG° Hairpin Kcal.mol^{-1}	ΔG° Self-Dimer Kcal.mol^{-1}
Amin-ssDNA-BHQ1	−5.64	−16.94
miR-21	−1.09	−6.6
Non-complementary	2.36	−3.61

Next, the hybridization free energy of perfect complementary and mismatched target sequences with molecular beacon probe was determined. Hybridization ΔG indicates the binding affinity of the two strands to a given probe to form a duplex. Moreover, this understanding has some practical consequences for optimal probe design. As shown in the Table S3, more negative ΔG° value, −35.09 kcal.mol^{-1}, was obtained for perfect complementary sequences hybridization which suggests a larger stable interaction.

Conclusions

A signal-on FRET nano-biosensor to monitor intracellular microRNA-21 using a CQD-based molecular beacon (MB) is reported. The CQD-based biosensor can detect very low amount of microRNA-21 in the sample with an acceptable selectivity and sensitivity. This CQD-based system has considerable benefits over organic dyes-based ones, for instance narrow and symmetrical emission spectra, particle size-tunable colors, exceptional stability and resistance to photobleaching. The CQDs are demonstrated to have a good aqueous solubility and very low toxicity to the cells. Thus, we suppose that this nano-biosensor has a great potential to be applied in microRNA-21 detection. The need for working with excitation wavelengths in the UV makes the probe prone to interferences by biomatter for both excitation and emission fluorescence.

Compliance with ethical standards The author(s) declare that they have no competing interests.

Publisher's note Springer Nature remains neutral with regard to jurisdictional claims in published maps and institutional affiliations.

References

1. Bhardwaj A, Singh S, Singh AP (2010) MicroRNA-based cancer therapeutics: big hope from small RNAs. Mol Cell Pharmacol 2(5): 213–219
2. Croce CM (2009) Causes and consequences of microRNA dysregulation in cancer. Nat Rev Genet 10(10):704–714
3. Bartels CL, Tsongalis GJ (2009) MicroRNAs: novel biomarkers for human cancer. Clin Chem 55(4):623–631
4. Liu L, Song C, Zhang Z, Yang J, Zhou L, Zhang X, Xie G (2015) Ultrasensitive electrochemical detection of microRNA-21 combining layered nanostructure of oxidized single-walled carbon nanotubes and nanodiamonds by hybridization chain reaction. Biosens Bioelectron 70:351–357
5. Wang F, Zheng Z, Guo J, Ding X (2010) Correlation and quantitation of microRNA aberrant expression in tissues and sera from patients with breast tumor. Gynecol Oncol 119(3):586–593
6. Goryacheva O, Mishra P, Goryacheva IY (2018) Luminescent quantum dots for miRNA detection. Talanta 179:456–465
7. Shi R, Chiang VL (2005) Facile means for quantifying microRNA expression by real-time PCR. Biotechniques 39(4):519–525
8. Várallyay E, Burgyán J, Havelda Z (2008) MicroRNA detection by northern blotting using locked nucleic acid probes. Nat Protoc 3(2): 190–196
9. Yin H, Zhou Y, Zhang H, Meng X, Ai S (2012) Electrochemical determination of microRNA-21 based on graphene, LNA integrated molecular beacon, AuNPs and biotin multifunctional bio bar codes and enzymatic assay system. Biosens Bioelectron 33(1): 247–253
10. Wen Y, Pei H, Shen Y, Xi J, Lin M, Lu N, Shen X, Li J, Fan C (2012) DNA nanostructure-based interfacial engineering for PCR-free ultrasensitive electrochemical analysis of microRNA. Sci Rep 2:867
11. Lim LP, Lau NC, Garrett-Engele P, Grimson A, Schelter JM, Castle J, Bartel DP, Linsley PS, Johnson JM (2005) Microarray analysis shows that some microRNAs downregulate large numbers of target mRNAs. Nature 433:769–773
12. Li W, Ruan K (2009) MicroRNA detection by microarray. Anal Bioanal Chem 394(4):1117–1124
13. Maroney PA, Chamnongpol S, Souret F, Nilsen TW (2008) Direct detection of small RNAs using splinted ligation. Nat Protoc 3(2): 279–287
14. Chen Z, Wang J, Miao H, Wang L, Wu S, Yang X (2016) Fluorescent carbon dots derived from lactose for assaying folic acid. Sci China Chem 59(4):487–492
15. Wolfbeis OS (2015) An overview of nanoparticles commonly used in fluorescent bioimaging. Chem Soc Rev 44(14):4743–4768. https://doi.org/10.1039/c4cs00392f
16. Molaei M (2018) A review on nanostructured carbon quantum dots and their applications in biotechnology, sensors, and chemiluminescence. Talanta. https://doi.org/10.1016/j.talanta.2018.12.042
17. Khakbaz F, Mahani M (2017) Micro-RNA detection based on fluorescence resonance energy transfer of DNA-carbon quantum dots probes. Anal Biochem 523:32–38
18. Hildebrandt N, Wegner KD, Algar WR (2014) Luminescent terbium complexes: superior Förster resonance energy transfer donors for flexible and sensitive multiplexed biosensing. Coord Chem Rev 273:125–138. https://doi.org/10.1016/j.ccr.2014.01.020
19. Geiβler D, Hildebrandt N (2011) Lanthanide complexes in FRET applications. Current Inorg Chem 1(1):17–35
20. Wang D, Hu L, Zhou H, Abdel-Halim E, Zhu J-J (2013) Molecular beacon structure mediated rolling circle amplification for ultrasensitive electrochemical detection of microRNA based on quantum dots tagging. Electrochem Commun 33:80–83
21. Tyagi S, Marras SA, Kramer FR (2000) Wavelength-shifting molecular beacons. Nat Biotechnol 18(11):1191–1196
22. Nawaz F, Wang L, Zhu L-f, Meng X-j, Xiao F-S (2013) Ascorbic acid assisted green route for synthesis of water dispersible carbon dots. Chem Res Chin Univ 29(3):401–403
23. Zhao Z, Zhang J, Wang Y, Chen L, Zhang Y (2016) Hydrothermal synthesis of fluorescent nitrogen-doped carbon quantum dots from ascorbic acid and valine for selective determination of picric acid in water samples. Int J Environ Anal Chem 96(14):1402–1413
24. Hu X, An X, Li L (2016) Easy synthesis of highly fluorescent carbon dots from albumin and their photoluminescent mechanism and biological imaging applications. Mater Sci Eng C 58:730–736
25. Zhu C, Zhai J, Dong S (2012) Bifunctional fluorescent carbon nanodots: green synthesis via soy milk and application as metal-free electrocatalysts for oxygen reduction. Chem Commun 48(75): 9367–9369
26. Liu S, Tian J, Wang L, Zhang Y, Qin X, Luo Y, Asiri AM, Al-Youbi AO, Sun X (2012) Hydrothermal treatment of grass: a low-cost, green route to nitrogen-doped, carbon-rich, photoluminescent polymer nanodots as an effective fluorescent sensing platform for label-free detection of cu (II) ions. Adv Mater 24(15):2037–2041
27. Yu P, Wen X, Toh Y-R, Tang J (2012) Temperature-dependent fluorescence in carbon dots. J Phys Chem C 116(48):25552–25557

28. Sun Y-P, Zhou B, Lin Y, Wang W, Fernando KS, Pathak P, Meziani MJ, Harruff BA, Wang X, Wang H (2006) Quantum-sized carbon dots for bright and colorful photoluminescence. J Am Chem Soc 128(24):7756–7757
29. Dong Y, Pang H, Yang HB, Guo C, Shao J, Chi Y, Li CM, Yu T (2013) Carbon-based dots co-doped with nitrogen and sulfur for high quantum yield and excitation-independent emission. Angew Chem 125(30):7954–7958
30. Sahu S, Behera B, Maiti TK, Mohapatra S (2012) Simple one-step synthesis of highly luminescent carbon dots from orange juice: application as excellent bio-imaging agents. Chem Commun 48(70):8835–8837
31. Lu J, Yang J-x, Wang J, Lim A, Wang S, Loh KP (2009) One-pot synthesis of fluorescent carbon nanoribbons, nanoparticles, and graphene by the exfoliation of graphite in ionic liquids. ACS Nano 3(8):2367–2375. https://doi.org/10.1021/nn900546b
32. Shan X, Chai L, Ma J, Qian Z, Chen J, Feng H (2014) B-doped carbon quantum dots as a sensitive fluorescence probe for hydrogen peroxide and glucose detection. Analyst 139(10):2322–2325
33. Contescu A, Contescu C, Putyera K, Schwarz J (1997) Surface acidity of carbons characterized by their continuous pK distribution and Boehm titration. Carbon 35(1):83–94
34. Tyagi S, Kramer FR (1996) Molecular beacons: probes that fluoresce upon hybridization. Nat Biotechnol 14(3):303–308